Chapter 3

RELATING STRUCTURAL INSULT TO VISUAL FUNCTION: SELECTED ACCIDENT CASES

Victoria Tepe, PhD*; James Ness, PhD†; and Bruce Stuck, ScD‡

*Senior Science Advisor, The Geneva Foundation, 917 Pacific Avenue, Tacoma, Washington 98402
†Colonel, Medical Services Corps, US Army; Professor of Discipline and Program Director of Engineering Psychology, Department of Behavioral Sciences and Leadership, US Military Academy, 601 Cullum Road, West Point, New York 10996
‡Formerly, Detachment Director; US Army Medical Research Detachment-Walter Reed Army Institute of Research, 7965 Dave Erwin Drive, Brooks City-Base, Texas 78235

Adapted from: Zwick H, Ness JW, Belkin M, Stuck BE. In vivo diagnostics and metrics in the assessment of laser-induced retinal injury. In: Friedl KE, Santee WR, eds. *Military Quantitative Physiology: Problems and Concepts in Military Operational Medicine.* In: Lenhart MK, ed. *Textbooks of Military Medicine.* Fort Detrick, MD: Borden Institute; 2012: 129–155.

INTRODUCTION

Laser-induced retinal injury is a function of both the nature of the laser exposure and the retina's acute and long-term response to the exposure. Conventional classifications of laser-induced retinal damage are based on acute laser-induced central retinal injury[1] with little attention given to secondary functional abnormalities that manifest as the effects of acute damage diminish. However, laser eye injuries associated with military laser fire-control (including rangefinding, designation, and illumination) systems have made evident the importance of suprathreshold laser-induced injury, revealing significant consequences for visual function even when laser-induced retinal damage is not restricted to the central retina.[2] Specific consequences involve the development of intraretinal scar formation (IRSF), associated retinal traction, and retinal nerve fiber layer (RNFL) damage. These secondary sequelae extend concern well beyond the macular region and, therefore, require new ophthalmic and functional techniques to assess their development, progression, and long-term consequences for visual function to distinguish normal functioning retina from dysfunctional retina.

The US Army Medical Research and Development Command and US Army Materiel Command established the Joint Laser Safety Team in 1968. Its mission was to study the nature and extent of potentially hazardous laser radiation emitted by military systems. A founding member of the team was Dr Harry Zwick, who dedicated his life's work to studying the relationship between laser exposure effects on the retina and the etiology of sequelae linked to changes in visual function. Together with the application of well-targeted functional assessment, advanced imaging techniques have enhanced the understanding of laser-induced retinal sequelae.[3] This chapter presents clinical evaluation of five military laser accident cases, representing a range of laser-induced retinal damage. These cases and evaluation techniques, first described by Zwick and his colleagues, were also featured in historical context to exemplify unique accomplishments and advances in the field of military quantitative physiology.[4] Each case underscores the complex relationship between structure and function and illustrates the importance of combining imaging techniques to precisely identify structural damage with well-targeted assessments to identify functional changes. These cases demonstrate that functional diagnostic tools should not be limited to examination of neural mechanisms that can be observed at the retina. As structural damage resolves, the processing of visual neural code along the visual pathway can lead to changes in visual function outcomes that are not immediately evident by observing the structural damage at the retina.

The next section of this chapter is an examination of imaging and visual techniques to assess retinal structure and visual function. Subsequent sections briefly explain how these techniques can be integrated to determine structural and functional relationships, as illustrated by each of the five presented accidental exposure cases included at the end of the chapter.

ASSESSING IN-VIVO RETINAL MORPHOLOGY

Confocal Scanning Laser Ophthalmoscopy

Confocal scanning laser ophthalmoscopy (CSLO) provides the capability for imaging the retina along its axial dimension, yielding image "slices" in eyes with relatively large focal lengths, from the anterior RNFL-dominated retinal surface posterior to the retinal vasculature.[5–8] Figure 3-1 shows CSLO images for a nonhuman primate (NHP) (Figure 3-1, a and b) and a garter snake (Figure 3-1, c and d). The graph reflects the current state of the art in axial domain resolution (18 μm) for eyes with relatively large focal lengths (eg, NHPs). The art of the possible in axial resolution is demonstrated in the garter snake eye, whose focal length is relatively short. For the NHP, however, the range of confocal slices is greater than for the snake eye. The optical properties of the NHP eye permit an axial range from the RNFL (see Figure 3-1a) to the retinal vasculature (see Figure 3-1b). The optical properties of the garter snake eye permit, by comparison, a narrower range of axial separation, which is from the RNFL (see Figure 3-1c) to the photoreceptor layer (see Figure 3-1d). However, the optical properties of the snake eye yield finer resolution of retinal structures than those of the NHP eye.

This comparative CSLO work, imaging eyes of species with differing optical properties, reveals the definitive advantage of imaging retinal elements and blood flow in the small eye. The small eye model allows for assessing damage to relatively fine retinal structure and for observing the repair cascade over time. New wave front correction techniques utilize adaptive optics algorithms to correct for optical aberrations of the imaged eye, allowing for diffraction limited imaging in the "large" human eye. Confocal applications now allow observation of the

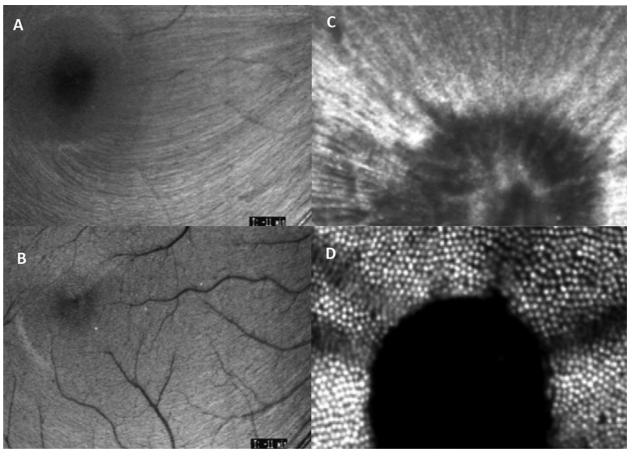

Figure 3-1. Comparison of range of confocal slice between rhesus monkey **(a,b)** and garter snake **(c,d)**.
Photographs: Courtesy of the Laser Laboratory, with the technical assistance of André Akers.

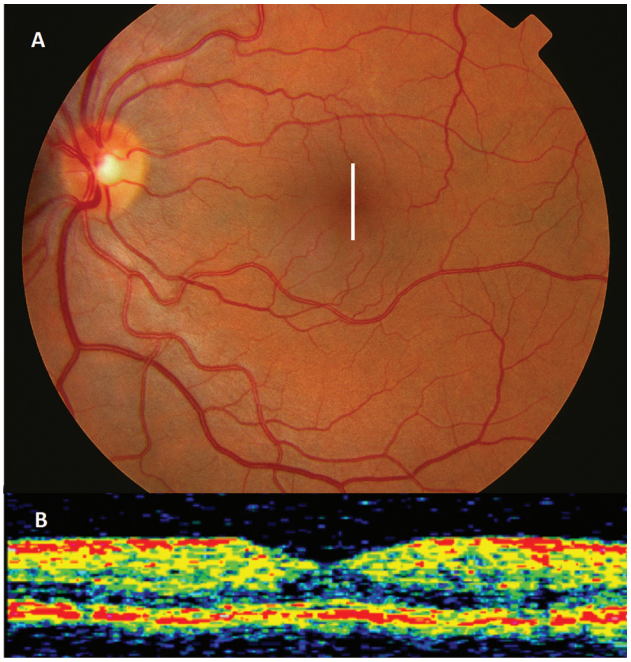

Figure 3-2. (a) Vertical scan through the fovea. **(b)** Optical coherence tomography image yields a full retinal thickness cross-section of scanned retina.
Photographs: Courtesy of the Laser Laboratory, with the technical assistance of André Akers.

photoreceptors and retinal pigmented epithelium in a human eye. These advances promise the detailing of morphological sequelae in the retina, from the RNFL to the retinal vasculature, to better understand and predict functional loss.

Optical Coherence Tomography

Optical coherence tomography (OCT) images provide an in vivo cross-section of the retina. Images are rendered in false color to indicate retinal layers and respective structures. Figure 3-2a shows the path of the OCT scan that rendered the image shown in Figure 3-2b. Figure 3-2, a and b, shows the OCT-rendered image taken through the macular region from superior parafoveal retina into foveal retina and ending in inferior parafoveal retina. The thickness of the parafoveal retina is 250 microns; the foveal retina, 150 microns. These thicknesses correspond with histological retinal measurements and thus can be used to characterize the condition of the retina.

FUNCTIONAL METRICS AND STRUCTURAL CORRELATES

Assessing Visual Function Along the Visual Pathway

High spatial resolution vision (ie, visual acuity) (VA) is mediated by the central foveal region.[9] VA demands a higher-order neural integration and augmentation, resulting in a relatively robust visual function. It is, therefore, not surprising that foveal retinal damage must be extensive, with a significant degree of secondary damage, to result in significant loss in VA. Maximal visual spatial resolution, measured as VA, is mediated at the center of the fovea. It was originally thought that center foveal ganglion cells innervated the most central region of foveal photoreceptors in a ratio of 1 ganglion cell to 1 photoreceptor,[10] resulting in an off-axis acuity function with a characteristic peak at the fovea and sharp declines in acuity with distance from the foveal axis.[11]

However, work by Curcio has shown that the central foveal cones have a 2:1 ratio with retinal ganglion cells.[12,13] When the 2:1 ratio is accounted for in the off-axis acuity function, it reveals a resulting small plateau of maximal acuity over the central foveal retinal space.[11] This structure-function relationship suggests that neural plasticity associated with central foveal cones may actually begin in the inner retina. At the inner retina, central foveal cone innervation with ganglion cells via Henle's fibers proceed to striate cortical visual space where the foveola (≈150 μm) is represented in a magnification of 7:1. In healthy visual systems, acuity provides a general measure of visual function. In laser accident cases where damage is confined to local areas of the retina, VA is often insensitive to associated visual function changes because

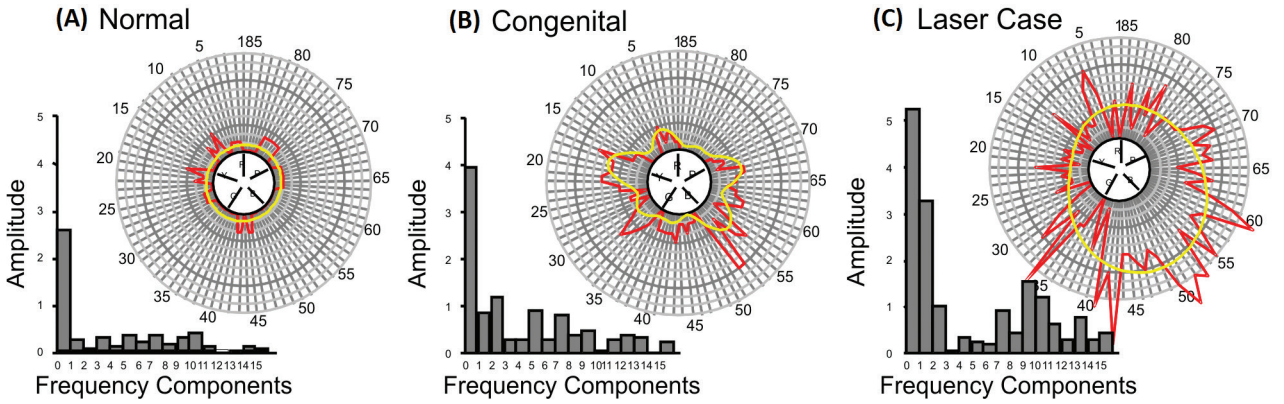

Figure 3-3. Farnsworth-Munsell (FM) 100 Hue test metrics for a human subject with normal color discrimination function **(a)**, a human congenital color deficient subject showing a bipolar deutan axis with a significant second-order Fourier frequency component **(b)**, and a human laser accident case **(c)** at 3 months postexposure showing a significant tritan monopolar error score and a highly significant first-order Fourier harmonic component. The axes of the FM 100 Hue test indicated in the center of the radial plots are B, blue; G, green; P, purple; R, red; and Y, yellow.
Illustrations: Courtesy of the Laser Laboratory, with the technical assistance of André Akers.

there is significant neural plasticity and redundancy associated with VA.

Contrast sensitivity, on the other hand, measures the reciprocal of the minimal contrast required (sensitivity) for detection of visual stimuli across spatial (size) or temporal (target flickered on/off) frequencies. Stimuli are modulated sinusoidally across light and dark bands subtending a specific visual angle in the spatial domain and across on/off cycles in the temporal domain. The spatial contrast function yields a relatively lower-order assessment of retinal integrity (magno/parvocellular ganglion cell systems) because higher-order processing of spatial information tends not to compensate for anomalies at the retina.[14] Further, evaluation of temporal sensitivity is important to characterize visual function changes or loss after laser-induced eye injury. Contrast sensitivity of the macular retina (targeting the more transiently responding magnocellular system involved in directing gaze) should be compared to the more sustained responding, centrally dominated parvocellular system.[15] In sum, the forms of the spatial and temporal contrast sensitivity functions provide a complete picture of threshold sensitivity across target size to register detection and movement predominately at the level of the retina.

As with VA, traditional clinical color vision metrics such as the Farnsworth Munsell 100 Hue (FM 100 Hue) are of limited utility because of their inability to accurately measure individual cone system damage. They involve measurements along the color (hue) discrimination dimension, which is not a direct measure of individual cone viability but, rather, is a measure of the neural reorganization of cone input that takes place in the inner layers of the retina.

The FM 100 Hue presents hues along the entire cycle of the color wheel. Given that the colors and their discrimination scores represent a position in the cycle of hues, one can pattern the data using frequency domain time series models.[16] Figure 3-3 shows the FM 100 Hue polar plots and their corresponding frequency density plots for a person whose vision is within normal limits (Figure 3-3a), a person with a congenital color deficiency (Figure 3-3b), and a laser accident case (Figure 3-3c).

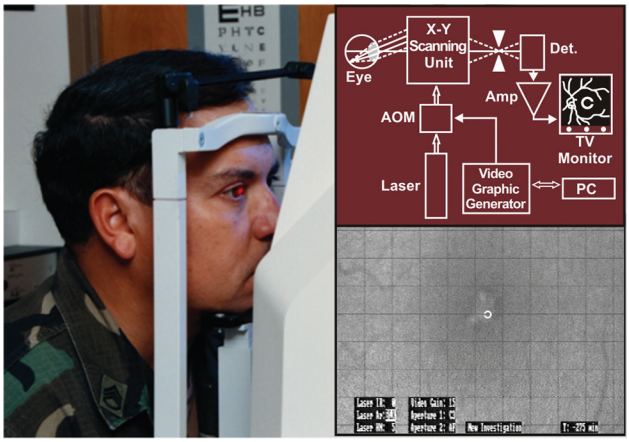

Figure 3-4. Confocal scanning laser ophthalmoscopy (CSLO) imaging of visual function test target placement on a patient's retina during measurement of contrast sensitivity. The schematic shows customized CSLO design, where Amp is amplifier, AOM is acousto-optic modulation, and Det is detector. PC is personal computer, and C is a Landolt C projected directly on the retina.
Photographs and illustration: Courtesy of the Laser Laboratory, with the technical assistance of André Akers.

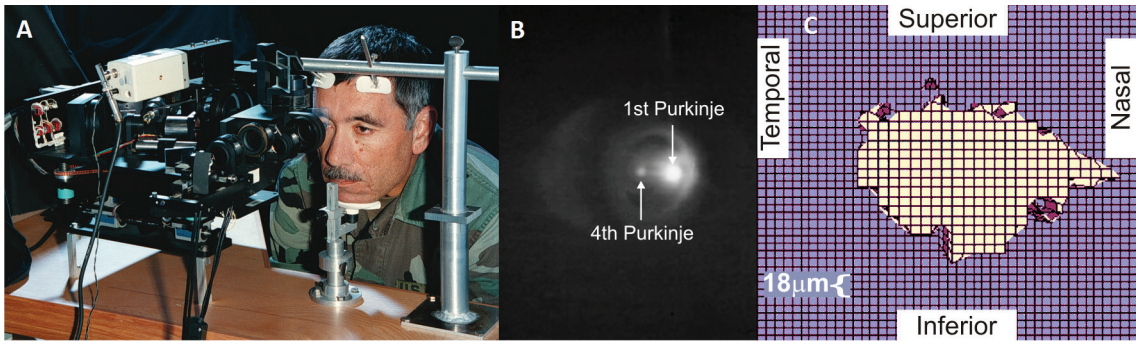

Figure 3-5. A normal eye movement map **(c)** acquired using a Stanford Research Institute (SRI) dual Purkinje eye-tracker (formerly, SRI International, Washington, DC; currently, Ward Technical Consulting, Jameson, Missouri) from a patient **(a)** who had reacquired normal fixation. The panel **(b)** shows the first and fourth Purkinje images, which are used to determine fixation to within 1 minute of arc and to differentiate eye rotation from head translation.
Photographs and illustration: Courtesy of the Laser Laboratory, with the technical assistance of André Akers.

The resultant frequency density plots from a Fourier transform reveal the content of the color vision error function along the color circle and quantify the relative contributions of the primary color deficit F1 and the primary deficit axis F2. F0 gives the average magnitude of error along the color circle. The remaining components are analogous to harmonics, suggestive of the magnitude of sequelae. Relatively symmetrical axis deficits are typical of congenital defects (see Figure 3-3b) with weak F1 contributions suggestive of a primary color deficit. In laser cases (see Figure 3-3c), significant F1 and F2 contributions exist. The F1 contribution suggests the extent of retinal alteration to cone types, and F2 suggests disruption of higher opponent processes.

The FM 100 Hue presents a focal target of color and, as such, may be less sensitive to outer retinal photoreceptor assessment of exposure effects that present with minimal ophthalmoscopic evidence of structural damage, but with subjective awareness of visual dysfunction. Under these conditions, several metrics involving outer retinal assessment have demonstrated the effectiveness of spectral sensitivity measures for VA criteria. These permit measurements of spectral sensitivity functions that are made sensitive to parafoveal and foveal retina by manipulation of spatial resolution (acuity) criteria ,[17,18] the development of color contrast grating techniques,[19] and the application of equal luminance color acuity charts.[20] The Rabin charts are especially notable in that they provide the capability to assess specific cone system functionality in the clinical environment. This capability could be applied to the current Aidman Vision Screener[21] with additional development and testing. The Screener was revised and now uses spectral Logmar acuity targets. Charts added to the Screener with and without neural opponent chromatic backgrounds may provide the capability of diagnosing laser exposure effects that present with minimal ophthalmoscopic evidence.

Integrating Imaging With Visual Function

Two separate techniques have been developed by US military medical researchers to assess the functionality of laser-damaged retinal sites. In the first technique, the CSLO raster pattern is modulated to provide a sufficient range of Landolt ring gap sizes (Figure 3-4). The technique is used to determine a contrast sensitivity function for local retinal areas. The operator can place the visual stimulus, via the CSLO raster, on areas of the retina that are of clinical interest and generate contrast sensitivity functions for those areas. In this way, the operator can interrogate morphologically anomalous regions suspected of laser-induced damage. This technique is particularly effective when the ophthalmoscopic evidence is equivocal, despite a visual complaint and suspected exposure.

A second technique utilizes normal fixation eye movement pattern technology[22] to evaluate individuals with laser-induced retinal damage. Such patterns have been shown to produce minimal visitation in retinal regions that are dysfunctional, thereby providing a "map" of functional and nonfunctional retina based on frequency of ocular motor visitation (Figure 3-5). Figure 3-5c shows the typical normal foveal fixation pattern. This pattern takes the general form of an ellipse, with the larger axis along the temporal/nasal extent, and typically spans an elliptical area of 150 x 100 microns. Deviations from this pattern are strongly associated with disruptions in the sensory system, which, in turn, disrupt the governing of the motor system directing eye movements.

LASER ACCIDENT CASES

The five laser retinal accident cases presented in this chapter all occurred in military settings and were all associated with laser-induced macular retinal hemorrhage. All cases were evaluated using techniques previously described. Four of the accidental exposures were induced by military laser rangefinders, and one was induced by a laser designator. Despite similarities in dose for the first four cases, lesion location was critical to outcome, but in ways not predicted by central versus peripheral convention. Case 5 was comparable to Case 4 in terms of lesion placement; this similarity highlights the importance of sensory-motor relationships, as well as the plasticity of the ocular sensory/motor system in reestablishing the visual system's ability to resolve fine-resolution targets.

Case 1

Case 1 received multiple accidental exposures to the right eye (OD) from an AN/GVS-5 laser rangefinder with an operating wavelength of 1064 nm at an energy output at the aperture of 15 mJ/pulse. The rangefinder was held at arm's length from the eye and delivered several pulses with an estimated total intraocular energy (TIE) of 2.0 mJ/pulse, which resulted in four retinal lesions, two of which produced vitreous hemorrhages. The TIE is the total energy incident on the cornea that can be transmitted through the pupil and can be focused on the retina. The TIE is not corrected for absorption and scatter through the outer ocular media. These two hemorrhagic exposures occurred nasal and temporal to the macula and a bridging scar though the foveal region was evident by 5 days postexposure.[23,24] Figure 3-6 shows the resulting intraretinal scar at 18 months postexposure.

Measurement of VA in the OD at 24 hours postexposure was 20/400, improving to 20/200 at 3 months postexposure. Measurements of VA for this case, made over a subsequent 2-year postexposure period, remained unchanged at 20/200 (OD) and in the unexposed eye at 20/20 ocular sinister (OS). Spatial and temporal contrast sensitivity measured at 6 months postexposure, using the CSLO technique already described, showed both high and low spatial frequency deficits. Figure 3-7 shows the maximum difference in spatial (stationary) and temporal (dynamic) contrast sensitivity between the OS and the OD. The spatial contrast sensitivity function shows the largest difference at approximately 4 cycles/degree, with the peak of the normal function at 6 cycles/degree. Furthermore, suppression for targets > 4 cycles/degree is greater than for targets < 4 cycles/degree. This indicates that there is significant disruption

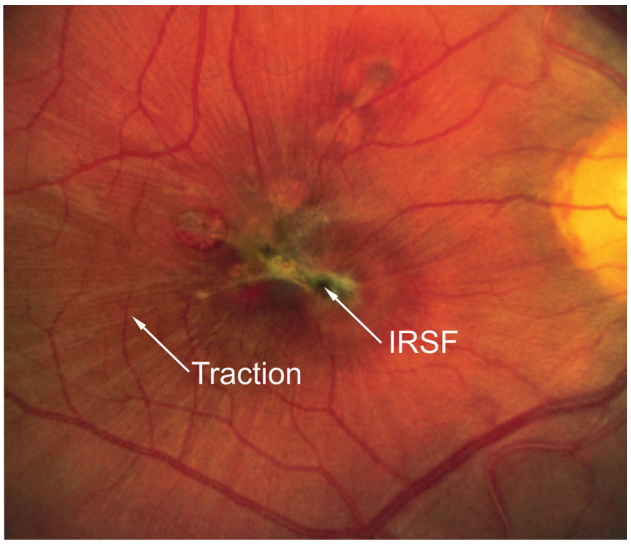

Figure 3-6. Case 1: Multiple exposures about the fovea and intraretinal scar formation (IRSF) between two of these lesion sites. Retinal traction extending from the IRSF is evident well beyond the macula.
Photograph: Courtesy of the Laser Laboratory, with the technical assistance of André Akers.

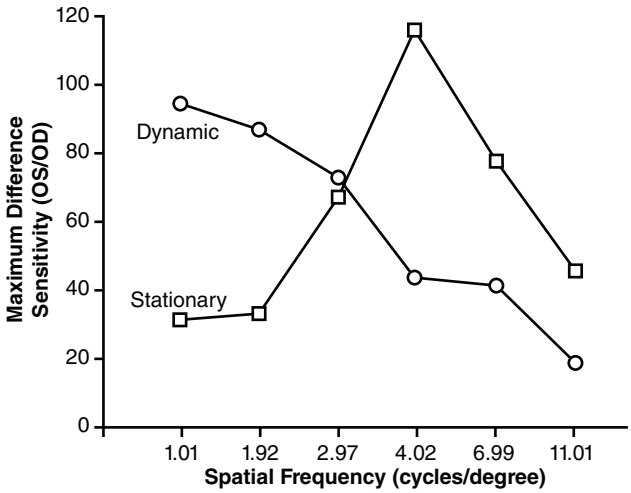

Figure 3-7. Measurements of stationary and dynamic contrast sensitivity (1-Hz luminance modulation) reveal maximum deficits in contrast sensitivity at 4 cycles/degree "Stationary" and 1 cycle/degree "Dynamic."
OD: right eye
OS: left eye
Illustration: Courtesy of the Laser Laboratory, with the technical assistance of André Akers.

to both magnocellular and parvocellular systems, with the magnocellular system disruption making a larger contribution to the overall visual function deficit.

The temporal contrast sensitivity function confirms the larger contribution of the magnocellular system disruption to the overall visual function deficit. The temporal contrast sensitivity function (see Figure 3-7, Dynamic) shows that for sinusoidal targets luminance modulated at 1 Hz, maximal deficit is at 1 cycle/degree. Under these measurement conditions, the typical temporal contrast sensitivity function peaks at 4 cycles/degree.[25] The fact that the largest deficit for spatial contrast was in the low- to mid-spatial frequency (4 cycles/degree) and that the temporal contrast sensitivity peak is shifted to the higher spatial frequencies (deficit is smallest at 11 cycles/degree) further confirms magnocellular system disruption. Note in the fundus photograph (see Figure 3-6) the extensive parafoveal traction, a secondary sequela from the tension caused by the contracting intraretinal scar. The traction may be contributing to the magnocellular system deficit since the magnocellular pathway arises principally from the parafovea.

Color deficits were assessed in the exposed eye (OD) with the FM 100 Hue test. Tests were performed 6 months subsequent to exposure and were given with and without fixation restrictions. Figure 3-8 shows the resolving of the color deficit from a large, average, relatively undifferentiated deficit weighted toward the blue to an average deficit that is within normal limits but, nonetheless, shows anomalies in the blue, green, and purple. Of note are the distinct clusters of frequency components for the restricted fixation conditions measure. The frequency component distribution shows a very large overall deficit (f0) and a strong unipolar component (f1), which is a strong blue weighting. The cluster of frequency components beyond f6 are indicative of the lack of a well-formed system to govern color discrimination, most likely the result of an inability to reliably fixate areas of the retina structurally intact enough to make a discrimination due to test-imposed fixation restrictions. When fixation restrictions were relaxed, the deficit resolved to a more well-formed frequency component distribution showing an overall deficit at f0, a weighting to the blue (f1) with differentiated green and purple contributing anomalies, and a nominal red pole (f4).

The persistence of the blue (S cone) anomaly across conditions is consistent with paramacular injury and magnocellular system disruption.[26] That is because medium and long wavelength-sensitive cones are concentrated almost exclusively in the fovea whereas short wavelength-sensitive cones are principally distributed parafoveally, and signals from these cones are carried by the magnocellular pathway. Thus, parafoveal damage impacts the chromatic system principally by disrupting the perception of blue and related hues. The color discrimination results are confirmatory of the contrast sensitivity results, indicating a strong magnocellular system disruption. Further, the fundus showed only paramacular lesions with the insult to the fovea due to the intrusion of an intraretinal scar. Visual field analysis did show functional central retina in the vicinity of the scar. Thus, when fixation restrictions for the FM 100 were relaxed, color discrimination improved to within normal limits, albeit with anomalies evident in the blue and related hues.

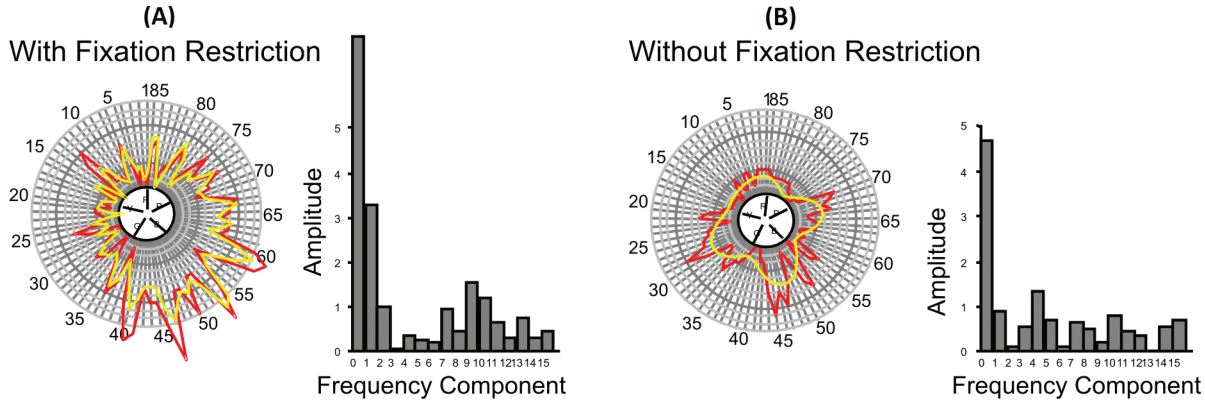

Figure 3-8. Farnsworth-Munsell (FM) 100 Hue scores for affected right eye (OD) show a shift from **(a)** a large fundamental indicating a large average error, with a strong first harmonic that is indicated in the graph as a strong blue deficit. This diminishes **(b)**, when fixation restrictions are relaxed, to an average error within normal limits although with significant first and fourth harmonic components. The axes of the FM 100 Hue test indicated in the center of the radial plots are B, blue; G, green; P, purple; R, red; and Y, yellow.
Illustrations: Courtesy of the Laser Laboratory, with the technical assistance of André Akers.

Case 2

Case 2 received bilateral accidental exposures from an AN/GVS-5 laser rangefinder with an operating Q-switched wavelength of 1064 nm with an energy output at the aperture of 15 mJ/pulse. The rangefinder was held about 0.6 m from the eyes and delivered at least two pulses with an estimated TIE of 1.0 mJ/pulse, which resulted in bilateral retinal lesions that produced macular holes. The focus of this case is the sequela observed in the OD over a 2-year period.

The OD received a paramacular exposure temporal to the optic disk and nasal to the macula in the papillomacular bundle (PMB). The lesion produced a vitreous hemorrhage in this region that took about 3 weeks postexposure to resolve. The lesion itself eventually developed into a full-thickness paramacular hole. Immediately following exposure, VA was 20/50 (OD); at 3 weeks postexposure, VA was 20/70 (OD); and by 13 months postexposure, VA deteriorated to 20/800 (OD) postsurgery. At 13 months, contrast sensitivity was not measurable beyond 6 cycles/degree.

Figure 3-9 shows the CSLO image of the paramacular hole and the CSLO image of the PMB–RNFL defect (Figure 3-9a) and an OCT scan through the center of the paramacular hole revealing complete loss of sensory retina (Figure 3-9b). The dotted outline shows the extent of retinal nerve fiber layer pruning in the region of the PMB showing a wedge defect. This particular defect was first described by Frische et al.[27] Zwick and colleagues later modeled the phenomenon in NHP to investigate the functional implications of the laser-induced retinal neural pruning that was shown to progress with Wallerian degeneration.[28]

Figure 3-9c shows the fixation eye movement patterns at 18 months after surgery to remove epiretinal scar tissue that was producing traction and inducing retinal detachment. The map of functional retina rendered by this technique allows for the assessment of functional retina from which to interpret the images of structural damage. Normal fixation eye movements map in an elliptical pattern, with the majority of visitation times within the fovea. The average extent of the nasal/temporal axis of the elliptical pattern is ≈150 μm and that of the superior/inferior axis ≈100 μm.[29] Comparatively, the fixation eye movement pattern shown in Figure 3-9c suggests a lack of strong sensory input to govern the eye movements. Although there appears some visitation in the area of the fovea, there is also a significant amount of searching around the functional boundary of the macular hole. Together, this suggests that the remaining sensory retina produces insufficient signal quality to govern target fixation. Note that the irregular shape of the boundary of functional retina and that the rendered map does not mirror exactly the size and shape of the hole. The functional map is dependent not only on the integrity of the neural elements, but also on communication between the sensory and motor systems. Thus, disruption in pathways will affect the functional map such that areas not visited in the eye movement map may appear relatively well formed in the

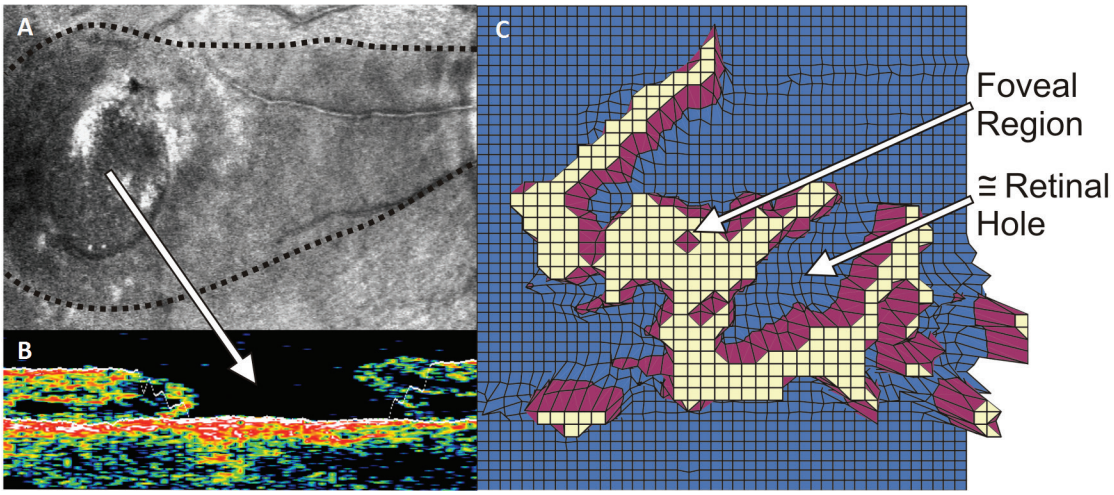

Figure 3-9. **(a)** Confocal scanning laser ophthalmoscopy image of a right eye (OD) paramacular hole taken after stabilization surgery at 18 months postexposure. The **dashed outline** shows the retinal nerve fiber layer defect. **(b)** Optical coherence tomography scan through this hole **(left white arrow)** shows loss of sensory retina, leaving retinal pigmented epithelium and choroidal vasculature. **(c)** Fixation eye movement map obtained for the OD postsurgery. Map shows a dysfunctional fixation pattern with fixation at any one location minimal. The grid is ≈400 × 400 μm; one grid square is ≈9 μm.
Photographs and illustration: Courtesy of the Laser Laboratory, with the technical assistance of André Akers.

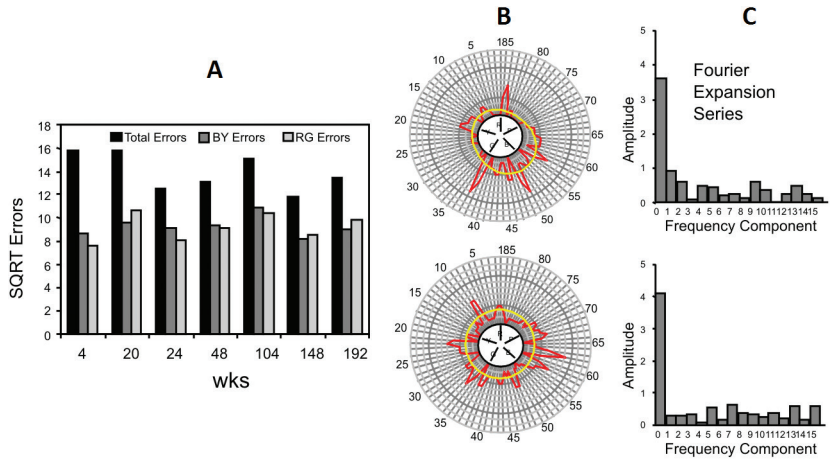

Figure 3-10. (a) Farnsworth-Munsell (FM) 100 Hue scores show no trends in total error scores. The frequency composition shows a transition in the distribution from **(b)** first harmonic contribution suggestive of a monopolar blue weighted deficit at 4 weeks postexposure to **(c)** a large f0 undifferentiated error at 192 weeks, suggesting an inability to discriminate color. The axes of the FM 100 Hue test indicated in the center of the radial plots are B, blue; G, green; P, purple; R, red; and Y, yellow.
BY: blue-yellow
RG: red-green
SQRT: square root
wks: weeks
Illustrations: Courtesy of the Laser Laboratory, with the technical assistance of André Akers.

structural imagery. The Wallerian degeneration of nerve fiber in the PMB can account for the differences between structural and functional imagery. Nonetheless, without the structural image showing nerve fiber track pruning, the functional map cannot be differentially interpreted.

Figure 3-10 shows FM 100 Hue color discrimination error scores over 192 days postexposure. There appears to be no trend in total and partial error scores, with all scores well beyond normal limits. The long-term absence of any significant harmonic frequency component indicates that the trichromatic receptor components have been equally affected (Figure 3-10c). This is most likely caused by the Wallerian neuronal degeneration observed in the PMB. These fibers transmit trichromatic cone output from the third-order neuron to higher brain regions that require this input for color discrimination.

Case 3

Case 3 received unilateral (OD) accidental exposure to a 1064 nm beam emitted by a battery-operated Nd:YAG laser rangefinder. The exit port of the rangefinder was held approximately 0.6 m from the eye. The eye received an estimated TIE of 2.5 to 3.0 mJ/pulse, which produced vitreal hemorrhage.[30] By 3 weeks postexposure, the vitreous hemorrhage had cleared. A full-thickness 100-µm diameter macular hole with evidence of traction was diagnosed at the 3-month postexposure fundus examination (Figure 3-11, a and b). An OCT image taken through the center of the lesion site (Figure 3-11c) revealed total loss of sensory retina in the macula hole and a significant choroidal extension beneath the fovea. Reflectance in the CSLO indocyanine green (ICG) image indicated vascular blockage (Figure 3-11d). ICG is a clinical imaging technique using dye to evaluate blood

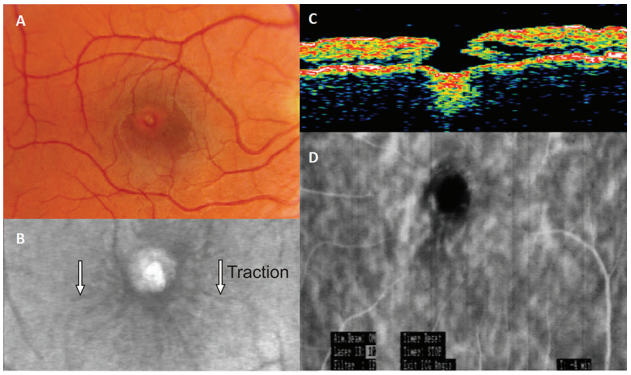

Figure 3-11. A full-thickness fundus photograph of the macular hole at 3 months postexposure **(a),** a corresponding confocal scanning laser ophthalmoscopy (CSLO) image showing evidence of traction **(b)**, an optical coherence tomography vertical scan through the center of the macular hole **(c)**, and a CSLO indocyanine green image with reflections indicating macula choroidal vasculature blockage **(d)**.
Photographs: Courtesy of the Laser Laboratory, with the technical assistance of André Akers.

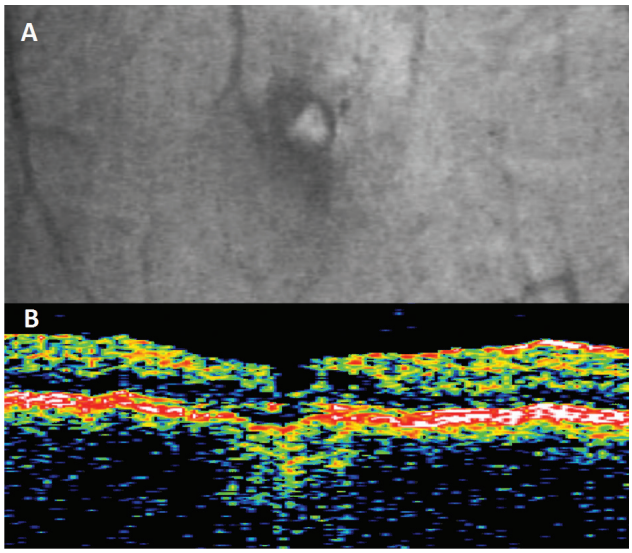

Figure 3-12. Macula hole diameter is reduced in size at about 12 months postexposure compared to 3 months postexposure (see Figure 3-11). **(a)** Confocal scanning laser ophthalmoscopy reveals an absence of retinal traction about the macular hole. Changes in choroidal entity appear weaker in reflectance at 12 months, but broader in extent. **(b)** Optical coherence tomography shows tissue bridging the gap of the macular hole. Photographs: Courtesy of the Laser Laboratory, with the technical assistance of André Akers.

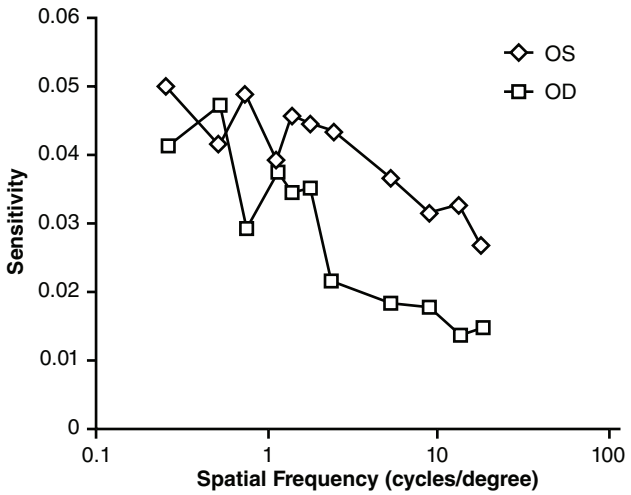

Figure 3-13. Contrast sensitivity, measured using the confocal scanning laser ophthalmoscopy technique, showed long-term right eye (OD) deficit in sensitivity for high spatial frequency visual stimuli. Note the significant suppression in OD sensitivity from 6–30 cycles/degree.
OS: left eye
Illustration: Courtesy of the Laser Laboratory, with the technical assistance of André Akers.

flow in the retina. At 12 months, CSLO images revealed a reduction in hole size and the disappearance of traction bands; changes in the choroidal entity appeared weaker in reflectance, but broader in extent (Figure 3-12a). The OCT showed evidence of tissue bridging the gap of the macular hole consistent with spontaneous reduction of the macular hole size (Figure 3-12b).

VA changed concomitantly with evidence of improvement in macular integrity. Upon presentation, VA was 20/150 (OD) and 20/20 (OS). At 3 weeks, VA improved to 20/60 (OD), then declined to 20/70 at 3 months, and improved to 20/40 by 12 months postexposure. Color discrimination FM 100 Hue functions were within normal limits at 12 months with no further change observed at 24 months postexposure. Contrast sensitivity measured using the CSLO technique showed a long-term deficit (OD) in sensitivity for high spatial frequency targets (Figure 3-13).

Fixation eye-movement patterns at 3 months were dominated by a vertical search pattern (Figure 3-14a). The vertical pattern spans an area greater than that of the foveal region. This pattern indicates a search for sensory retina to attract fixation eye movements. At 3 months postexposure, focal areas of the functional sensory retina were unable to produce a strong enough signal to govern eye movements. At 12 months postexposure, the fixation eye movements showed an attraction focus and the development of a significant horizontal component. This component spans the typical ≈150 μm extent. However, the persistence of the vertical component suggests the signal attracting eye movement visitations is weak (Figure 3-14b).

Case 4

Case 4 received bilateral accidental exposures from an AN/GVS-5 laser rangefinder with an operating Q-switched wavelength of 1064 nm, producing an energy output at the aperture of 15 mJ/pulse. The rangefinder was held about 0.6m from the eyes and delivered at least two pulses with an estimated TIE of 1.0 mJ/pulse, which resulted in bilateral retinal lesions that produced macular holes. The focus of this case is on the sequelae observed in the OS over a 2-year period.[31]

The OS suffered an acute macular vitreous hemorrhage with long-term damage restricted to the fovea. Figure 3-15 shows a fundus (Figure 3-15a) and CSLO image (Figure 3-15b), demonstrating a discontinuity through the center of the fovea. Figure 3-15c shows an OCT image revealing the extent of a small, flat macular hole through the center of the fovea.

VA at 48 hours postexposure was 20/200; by 8 days postexposure, VA improved to 20/25; and by 3 years postexposure, VA improved to 20/15. Color

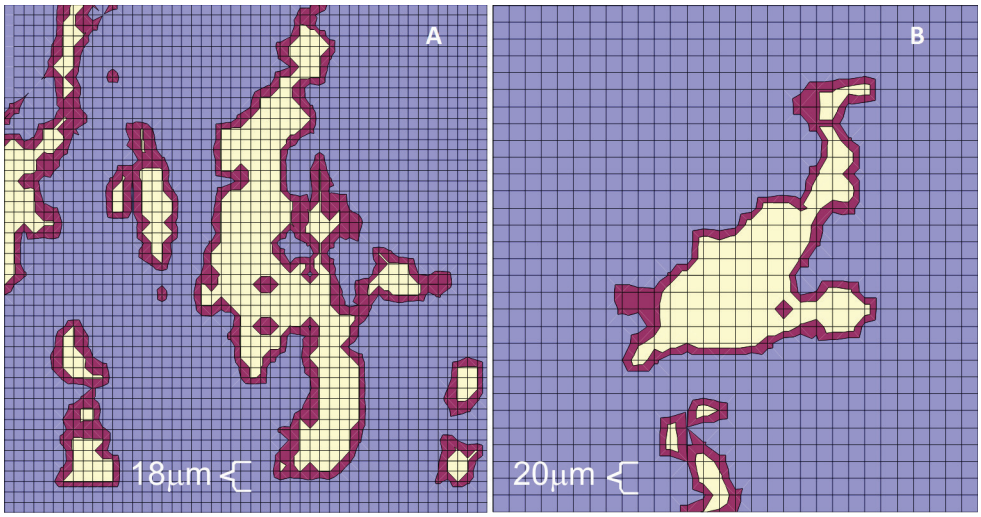

Figure 3-14. Fixation eye movements changed significantly from 3 **(a)** to 12 **(b)** months postexposure. At 3 months, an atypical vertical movement was observed that spanned over a 300-μm vertical range with little horizontal movement. At 12 months, fixation eye movements show a definite focus and a more typical horizontal extent **(b)**.
(Scale a: 1 box = 6 μm; Scale b: 1 box = 10 μm)
Illustrations: Courtesy of the Laser Laboratory, with the technical assistance of André Akers.

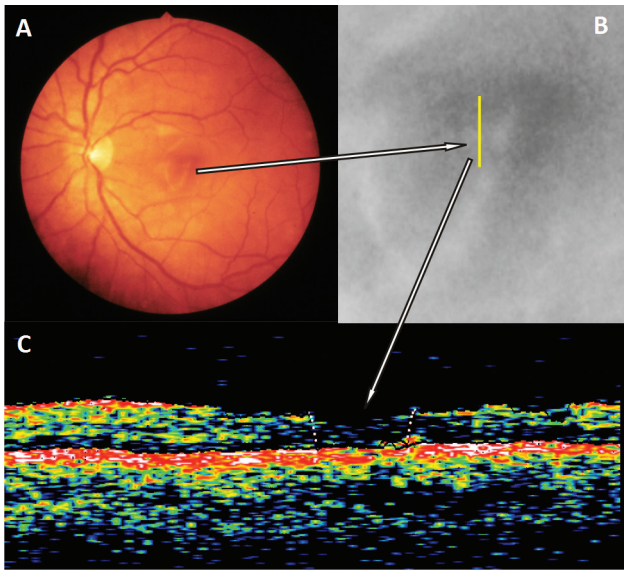

Figure 3-15. The fundus photograph **(a)** shows a central anomaly in the macular area (**note light spot** in the center of the typical darker central macular area). The confocal scanning laser ophthalmoscopy image shows a small foveal break in the retina and the track of the optical coherence tomography (OCT) scan across the break **(b)**. The OCT image shows a small, flat central hole **(c)**.
Photographs: Courtesy of the Laser Laboratory, with the technical assistance of Andre' Akers.

discrimination measured with the FM100 Hue test at 3 years postexposure demonstrated error scores within normal limits, with no significant axis or harmonic components.

Landolt ring contrast sensitivity measured under CSLO retinal observation confirmed that foveal placement was not used in discriminating small Landolt ring targets normally requiring foveal utilization. Instead, such targets were consistently placed superior and slightly temporal to the fovea. The contrast sensitivity function peaked at the typical 6 cycles/degree, and sensitivity across spatial frequency was within normal limits although at the lower limit (Figure 3-16).

At 4 years postinjury, VA was recorded at 20/15. Figure 3-17 shows the fixation eye-movement patterns at this time, the focus of which is consistent with that of the earlier CSLO observation (Figure 3-16a). The focus of the fixation eye movements tracks along the superior boundary of the foveal hole. The map of the eye movements about a focus superior and slightly temporal to the anatomical fovea shows a pattern typical of healthy eyes, indicating the formation of a psuedofovea.[32] The eye movement map also shows visitations outlining the extent of nonfunctional fovea, which corresponds to the size and shape of the hole identified in the fundus examination. This case provides functional support to Curcio's structural findings[12,13] and suggests that the VA function peak corresponding to the foveola (≈150 μm) is most likely a result of its visual cortex representation, which is magnified at a ratio of 7:1.[11]

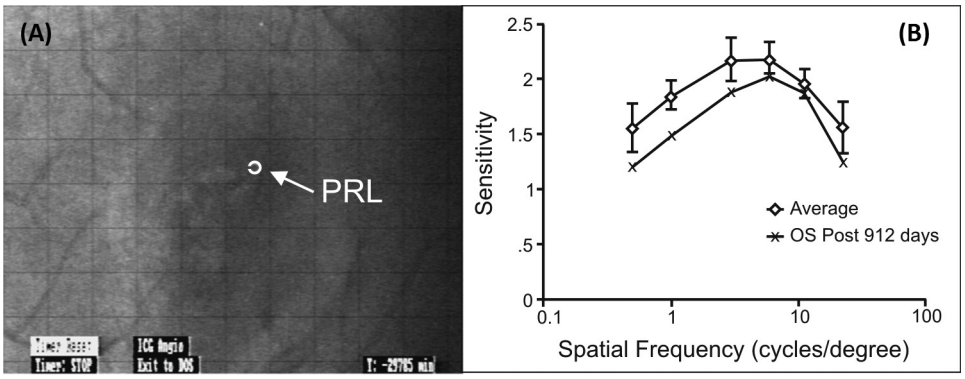

Figure 3-16. The confocal scanning laser ophthalmoscopy image shows contrast sensitivity test for the preferred retinal location (PRL) for resolving fine-resolution targets **(a)**. The placement of fine-resolution targets is superior and temporal to the fovea. Contrast sensitivity at 912 days postexposure shows a contrast sensitivity function within—although at the lower limit of normal **(b)**.
OS: left eye
Photograph and illustration: Courtesy of the Laser Laboratory, with the technical assistance of André Akers.

Case 5

Case 5 received bilateral accidental exposures from a Q-switched Nd:YAG laser designator, which emitted 10 laser pulses/second at a wavelength of 1064 nm. The exit beam diameter (10 cm) was large enough to permit a simultaneous bilateral exposure. Eye position at exposure was a few centimeters from the exit aperture with a received TIE estimated at 315 μJ/pulse. The exposure induced confined bilateral macular hemorrhages. The hemorrhage was slightly larger in the OD and centered on the fovea. The patient was treated within 6 hours postexposure with a moderate steroid dose, and a taper continued for a postexposure period of 2 weeks.[33] This case describes sequelae in the OD.

Figure 3-18 shows the laser designator and a reconstruction of the bilateral exposure scenario. At 4 days postexposure, OCT imaging showed a fovea with a break in retinal pigment epithelium (RPE) integrity beneath the fovea. At 1 month, the RPE break resolved to minimal foveal thickness. Foveal thickness at 4 months showed significant thickening close to the normal foveal thickness and was accompanied by a return of normal color discrimination, VA, and contrast sensitivity within this same 4-month time frame. In the third column of images, corresponding CSLO images are shown, revealing a reduction in the lesion size from 2 days to 1 month and the disappearance of an ophthalmoscopically visible lesion by 12 months postexposure.[34]

VA at 3 hours postexposure was 20/50 (OD) and diminished to 20/200 (OD) by 2 days postexposure. VA recovered to normal levels within 3 months postexposure. Color discrimination was nominally beyond normal limits at 2 days postexposure. At 1 month postexposure, color discrimination functions were within normal limits, as measured with the FM 100 Hue examination.[34] Landolt ring contrast sensitivity functions measured under CSLO visualization at 4 days postexposure showed

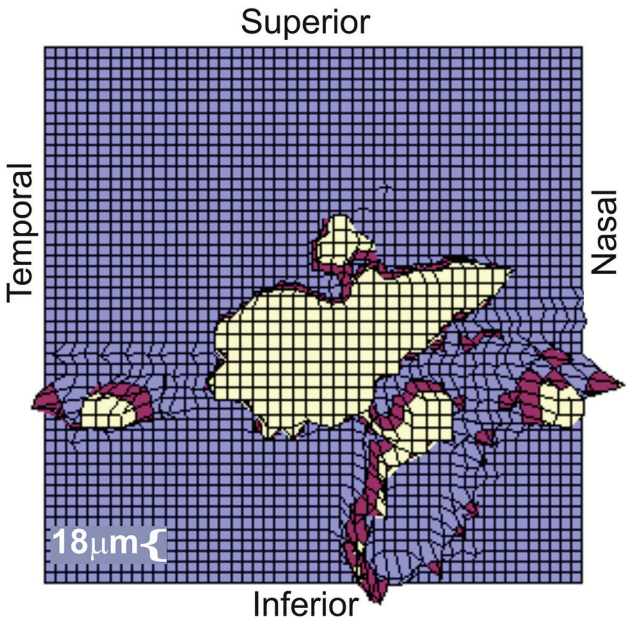

Figure 3-17. Fixation eye movements recorded at 4 years postexposure for fine-resolution targets. The pattern confirms the earlier finding with confocal scanning laser ophthalmoscopy showing, in relation to the fovea, a superior/temporal fixation locus. Other than the shift in locus and visitation along the boundary of the hole, the fixation pattern is typical of those seen in healthy eyes.
Illustration: Courtesy of the Laser Laboratory, with the technical assistance of André Akers.

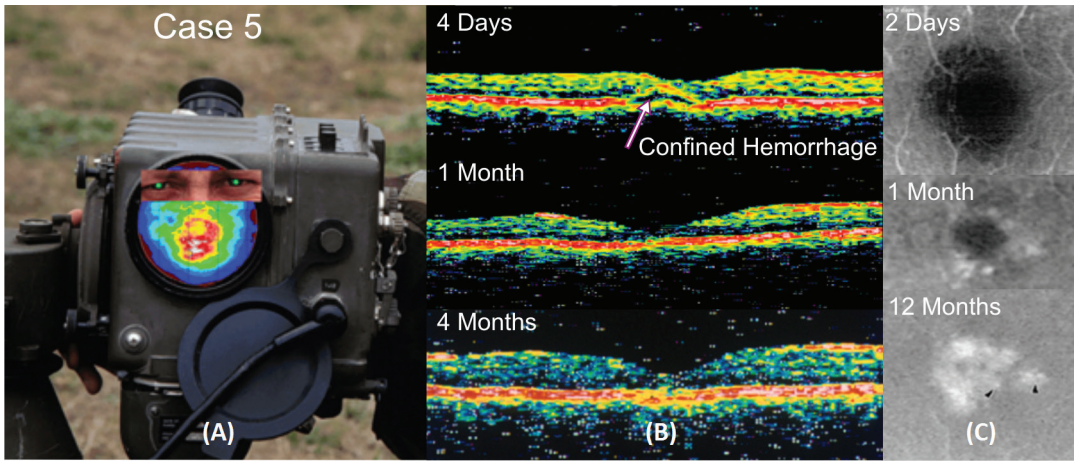

Figure 3-18. The large exit port of the designator makes it possible for bilateral exposure at ocular distances of a few centimeters **(a)**. Optical coherence tomography **(b)** images show the progression of right eye wound healing from 4 days through 4 months and confocal scanning laser ophthalmoscopy **(c)** images from 2 days through 12 months postexposure.
Photographs: Courtesy of the Laser Laboratory, with the technical assistance of André Akers.

uniform suppression, with peak sensitivity shifted from the typical 6 cycles/degree mid-spatial frequency peak to a peak at 1 cycle/degree. The peak shift to lower spatial frequencies indicates a disruption in foveal function. At 9 months, contrast sensitivity functions were within normal limits and corresponded to a shift in preferred retinal location (PRL) from fixation superior and slightly temporal to the fovea to within the fovea (Figure 3-19a). Figure 3-19b shows that fixation eye movements at 9 months are consistent with typical, human-fixation eye-movement patterns.[22] The map shows no functional disruption within the foveal region.

REVIEW

Five laser injury cases involving retinal hemorrhage were evaluated with ophthalmic techniques that related structural insult to visual function. The cases' results indicate the complexity of the structure-function relationship and the scope of visual system resilience (Table 3-1). Despite similarities in dose, placement of the lesion on the retina contributed significantly to visual function outcome, but not in a classically expected manner. For example, Cases 4 and 5 demonstrate that foveal damage does not equate to diminished VA in that foveal-like function can be recovered through a shift in PRL from the fovea to a position superior and slightly temporal to the fovea.[35]

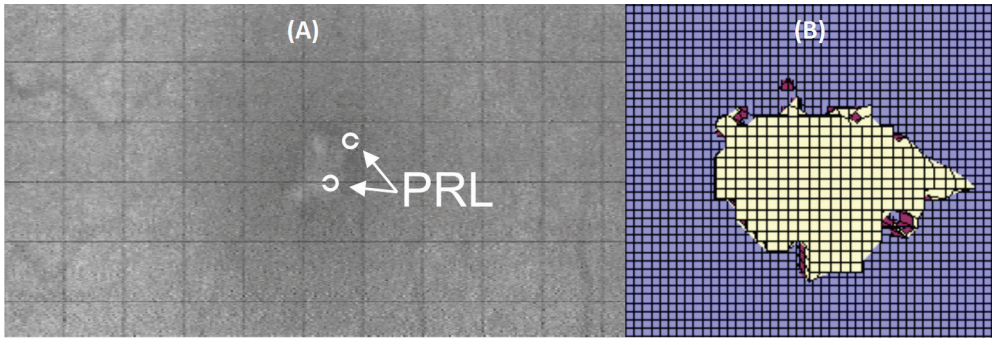

Figure 3-19. The confocal scanning laser ophthalmoscopy image shows the shift in preferred retinal location (PRL) for placing fine-resolution targets (<10 cycles/degree) from a focus superior/temporal to the fovea to a focus within the fovea **(a)**. With the PRL return to the fovea, the fixation eye movement map **(b)** shows a typical pattern, with no indication of residual functional damage.
Photograph and illustration: Courtesy of the Laser Laboratory, with the technical assistance of André Akers.

TABLE 3-1

SUMMARY OF CASE FINDINGS

	Dose TIE mJ	Injury Initial	Hemorrhage	Visual Acuity Initial	Visual Acuity Resultant	Contrast Sensitivity Resultant	Color Discrimination Resultant	Ocular Motor	Resultant Secondary Sequelae
Case 1	2.8	4 Paramacular retinal lesions; 2 producing macular holes	2 Paramacular holes produced vitreous hemorrhage	20/400	20/400	Significant overall suppression peak shift to 10 c/d	Overall disruption, blue axis most prominent	Some functional central retina in vicinity of scar	Retinal scar between paramacular holes bridging macular and associated traction
Case 2	1.0	Full-thickness paramacular hole; temporal to optic disc, nasal to macular in PMB	Vitreous hemorrhage	20/50	20/800	Not measurable beyond 6 c/d	Uniform suppression with no dominant axis	Atypical vertical scan pattern with no dominate retinal site attracting eye movement	Considerable nerve fiber degeneration in PMB, with evidence of Wallerian degeneration to the optic nerve
Case 3	2.5–3.0	Full-thickness 100 μm diameter center macular hole	Vitreous hemorrhage	20/150	20/40	Significant suppression in sensitivity OD from 6 to 30 c/d	WNL	Significant typical horizontal scan with persistence of atypical vertical component	Reduction in hole size and disappearance of traction bands
Case 4	1.0	Small, flat macular hole through the center of the fovea	Vitreous hemorrhage	20/200	20/15	Contrast sensitivity function within, although at the limit of normal	WNL	Superior/Temporal to fovea fixation with typical movement pattern	No change in initial injury
Case 5	0.315	Break in RPE integrity beneath the fovea	Confined macular hemorrhage centered in fovea	20/50 OD at 3 hours and 20/200 at 2 days post	20/15 OU at 10 months and 20/25 OU at 14 months, OD not recorded	Recovered from uniform suppression with peak sensitivity; shifted to 1 c/d to a function within normal limits	WNL	PRL shift from superior/temporal back to fovea	Treated with steroid; significant thickening close to the normal fovea thickness

(Table 3-1 *continues***)**

Table 3-1 *continues*

c/d = cycles per degree
mJ – millijoule
OD = right eye
OU = both eyes
PMB = papillomacular bundle
PRL = preferred retinal location
RPE = retinal pigmented epithelial layer
TIE = total intraocular energy
μm = micrometers
WNL = within normal limits
Adapted from Zwick H, Ness JW, Belkin M, Stuck BE. In vivo diagnostics and metrics in the assessment of laser-induced retinal injury. In: Friedl KE, Santee WR, eds. *Military Quantitative Physiology: Problems and Concepts in Military Operational Medicine*. In: Lenhart, MK, ed. *Textbooks of Military Medicine*. Falls Church, VA: Department of the Army, Office of The Surgeon General, Borden Institute; 2012: 129–155.

Structural damage was detailed through the utilization of CSLO and OCT imaging techniques that demonstrated the depth of IRSF and RNFL-PMB damage in vivo, confirming previous NHP histological studies of these secondary damage processes.[30] CSLO imaging demonstrated that retinal traction exists above the RNFL and often may extend into the vitreous, possibly altering normal photoreceptor orientation, which has been demonstrated to cause reduction in visual sensitivity.[36]

Spatial visual function metrics of VA and contrast sensitivity are seriously affected by retinal traction and IRSF. These damage mechanisms alter receptor orientation of large retinal areas, reduce retinal thickness, and induce neural disorganization in the process of their formation. Case 1 showed the most serious example of traction and IRSF effects on spatial vision metrics, affecting both stationary and dynamic measures of contrast sensitivity associated with the global effects of IRSF and traction. Failure of acuity to recover over the 2-year period is also significant, as acuity is highly "protected" by cortical magnification of the fovea (relative to the parafoveal region) and by findings that indicate neural receptor field plasticity or expansion that provides added neural redundancy for reduced foveal retinal neural output.[37]

The mechanism that prevents neural plasticity in Case 2 is associated with the interruption in the PMB region of the RNFL caused by induction of the paramacular hole that formed following resolution of vitreous hemorrhage. Evidence that the fovea was still functional, but could not transmit its spatial and chromatic neural output to higher-order visual brain systems was supported by fixation eye movement maps demonstrating foveal visitation capability. While this lesion was parafoveal, and ordinarily such lesions are given less importance than more central retinal lesions, this particular lesion interrupted the major neural pathway carrying foveal neural retinal code to higher-order brain mechanisms.

In the absence of secondary damage mechanisms previously described, spatial and chromatic vision may recover over a time span of about 3 to 6 months, as seen in Cases 4 and 5. The surprising release of traction in Case 3 and the ensuing full recovery of color discrimination and near complete recovery of VA was unexpected, but documented by the capability of CSLO imaging to capture anterior retinal pathology. Nevertheless, while acuity continued to recover, presumably via cortical neural compensation for reduced foveal receptor output, contrast sensitivity remained constant, showing a consistent deficit in the high spatial frequencies. This is indicative of the strong association between contrast sensitivity and lower-order retinal ganglion cell systems.[38] On the other hand, the rapid recovery of color discrimination to normal levels at 12 months may relate to the fact that color vision photoreceptor systems are distributed over broader regions within the fovea, where photoreceptor to ganglion cell ratios are larger than those in the central fovea.[39]

A critical factor in understanding the mechanism of neural plasticity in Case 4 is the observation made with the OCT that showed a "break" in the central foveal region. This break may have caused some degree of failure in normal foveal function, resulting in a degree of dysfunction in spatial vision and PRL replacement neural mechanisms. Evidence for this hypothesis was observed in both the development of a new PRL superior and slightly temporal to the fovea and in the fixation eye movements for fine-resolution targets as mapped with the dual Purkinje eye tracker. The latter confirmed the establishment of a new PRL and further showed optical accommodation with this shift of about 0.25 diopters, sufficient to produce a baseline acceptable point spread function.[29]

Case 5 initially showed a PRL superior and slightly temporal to the fovea, identical to that of Case 4. However, during this 3- to 6-month postexposure period, other visual functions—including VA and sine wave contrast sensitivity—were still recovering. During this recovery period, CSLO Landolt ring contrast sensitivity showed frequent, but not sustained, placement of Landolt ring contrast sensitivity targets within the fovea, prognostic of the recovery of foveal function. This function did recover between 6 and 9 months postexposure. Color discrimination, measured with the FM 100 Hue examination, had recovered in both eyes within the first month postexposure, indicating that cone mechanisms had recovered or were sufficiently active to minimize possible residual selective cone dysfunction. This is most likely due to a greater

inherent redundancy of the cone-to-ganglion cell ratio in the foveal regions and further magnification of this relationship to the visual cortex.

At nonhemorrhagic levels, metrics that evaluate outer retinal cone system functionality appear to be more sensitive than those that rely on achromatic metrics of VA and not on contrast sensitivity.[17] When accidental exposure is repeated by malfunction[19] or by intentional exposure,[40] functional loss in spatial retinal-based metrics may become permanent, although high-contrast achromatic VA may still be compensated by static or dynamic visual cortex plasticity. Of special note is the color contrast examination developed by Arden et al that uses both color opponency and color contrast.[19] These metrics interrogate both retinal ganglion cells as well as higher-order visual processing that render contrast, color opponency, and color contrast information. While this test represents a major advance in utilizing various levels of neural code arising from the retina, this test could also be improved to track the neural code arising from the fovea by utilizing a broader range of spatial frequencies in evaluation of retinal systems associated with central fovea visual function.[18]

Finally, the animal behavioral and morphological evaluations of outer retinal cone function require some discussion. Sperling et al demonstrated the photic toxicity of short-wavelength light to S cone photoreceptors and that such exposures occurred in the range of 5 $\log_{10}$ Td.[41] This brightness level is slightly higher than comfortable brightness, but not considered a thermal threat. However, prolonged exposure to such levels of highly monochromatic blue light did produce permanent deficits in S cone incremental spectral sensitivity, indicating vulnerability of either the S cone or some other component in the retina sensitive to such visible radiation.[42]

Reidenbach et al reported a persistent afterimage lasting 108 hours after exposure to a 405-nm source at a cumulative TIE of 3.813 mJ.[43] In total, there were nine exposures, each 1 second in duration, at increasing power from 1 nW to 560 μW in a trial series with a cumulative TIE of 1.27 mJ per series. Three trial series of exposures were delivered over a 2-hour period to allow time for visual recovery before each subsequent exposure. Retinal illuminance for the 560-μW exposure was about 6.88 $\log_{10}$ Td. As reported by Ness et al (see Chapter 6, The Effects of Nondamaging Levels of Laser Energy on Vision and Visual Function), the 405-nm exposure is more than two orders of magnitude less than that of Stamper et al,[44] who exposed volunteers to a 514.5-nm source at 9.23 $\log_{10}$ Td retinal illuminance, producing an afterimage that lasted no more than a minute. These exposures are well below the maximum permissible exposure level, yet the 405-nm exposure had a profound effect on vision. Zuclich reported damage threshold for near-ultraviolet (UV) at 0.28 J.[45] The cumulative TIE reported by Reidenbach et al was 0.0038 J.[43] Given the multiple exposures, the possibility of a phototoxic conditioning effect may have occurred.[46] Taken together, the research supports the phototoxic effect of near-UV on S cones as reported by Sperling et al.[41] This issue has taken on greater relevance with the discovery of third harmonic effects from pulsed 1.3-micron laser systems.[47]

The experiments of Zwick[3] and Schmeisser[48] bring another aspect to this review, which is the possibility that the unique interference patterns (speckle) induced by visible laser light when irradiating a surface may have peak powers high enough to produce significant retinal dysfunction or photoreceptor loss. While this hypothesis remains to be validated, it should be pointed out that higher-order brain mechanisms continue to form complex methods of producing images from unique neural signals and that prolonged viewing of speckle with moderate peak powers above average power may induce neural reorganization in ways that may degrade visual function. Parallel exposures made on NHPs revealed unique histopathological findings of increases in basal bodies and striated rootlets within the RPE that indicate significant physiological changes can be induced by such exposure.[49] These changes may have been responsible for detuning receptor systems associated with high acuity criteria and sensitizing receptor systems at lower acuity criteria; however, over about a 2-year period, receptor systems appear to have been reorganized with peaks and levels of sensitivity consistent with those of higher-acuity spectral sensitivity functions. These observations are consistent with similar long-wavelength cone system emergence following acute foveal injury to small spot Q-switched 690 nm dye laser exposure,[3] suggesting that such effects may be triggered by a wide range of laser energy exposure levels.

The ability to address the diagnostic issues reviewed in this chapter with an animal model capable of providing an in vivo view of such processes in "action" is unique. In vivo imaging of laser-induced retinal injury and repair processes has shown changes in the internal reflection of photoreceptors, indicative of changes in mode structure.[50] Changes in mode structure suggest a change in photoreceptor orientation and, thus, in sensitivity to particular spectral frequencies.[51] Such reflectivity is not the same as a lesion observed in a large eye (eg, NHP) because of the full thickness and low resolution with respect to cellular structure in the large eye. The in vivo small eye model is also different from histological preparations because it exists in its natural

state within the retina. The behavior of the in vivo small eye model can be documented to include changes in orientation, reflectivity, and migration into the center of a laser retinal injury site. The latter has been suggested as a retinal plasticity mechanism and documented by retinal photoreceptor histology, suggesting that, over time, peripheral photoreceptors may migrate into lesion sites clear of damage photoreceptors.[52] The importance of this observation relates to the fact that, in the NHP and human retina, damaged photoreceptors in the fovea are dominated by cones. If migration is a relevant explanation of visual functional recovery, replacement receptors from the peripheral retina must have characteristics that provide trichromatic cone characteristics. Such characteristics may simply be greater redundancy, as in Case 5 for return of color discrimination. However, long-wavelength cone emergence was also demonstrated over very different spectral and energy levels. This suggests that the reemergence of long-wavelength cone systems may involve unique photoreceptor spectral tuning, requiring an active rootlet system within the photoreceptor and the RPE, to provide a range of movement parameters that might be necessary for such spectral tuning of the waveguide.[53]

SUMMARY

In this chapter, metrics that combine structural and functional diagnostic techniques revealed a wide variety of damage and recovery processes. These techniques are needed for reliable, rapid, and valid measures of visual function deficits associated with laser retinal injury. Further development will be needed as lasers become smaller, more spectrally agile, and more widespread. Techniques are needed to interrogate the full spectrum of visual function, including the contrast required to resolve features that subtend a range of visual angles, the ability to detect fine differences in hue, and the sensory-motor coordination of fixation eye movements. Until deficits in these functions are diagnosed, researchers are limited in their ability to evaluate the functional consequences of laser retinal injuries and differentiate changes that are primarily retinal in origin from higher-order sequelae. In the military situation, rapid differential diagnostic procedures are required to identify laser-induced retinal injury. These procedures will require compact ophthalmoscopes with axial, as well as transverse, retinal imaging capability with integrated visual function tests that interrogate the span of visual processing from the retina into higher-order visual centers. This investigative functionality will allow for the identification of vision loss that may be due to retinal or brain physiological dysfunction.

As adjunct to other military systems, and possibly as weapons in their own right, lasers will continue to play an important and sometimes dangerous role on the modern battlefield. At present, there is no adequate comprehensive protection against accidental or intentional exposure to lasers in combat. Thus, it is critical that the field of laser safety research move forward toward the development of preventative protocols and prophylactic technologies to protect military personnel and to support military operational objectives.

Acknowledgments

The authors acknowledge the memory of Harry Zwick, with gratitude to him and his colleagues for their previous work in this area. Special thanks also to the US Army Medical Research Detachment-Walter Reed Army Institute of Research Laser Laboratory and, in particular, André Akers for images, illustrations, and technical assistance.

REFERENCES

1. Wolfe JA. Laser retinal injury. *Mil Med.* 1985;150:177–185.

2. Barkana Y, Belkin M. Laser eye injuries. *Surv Ophthalmol*. 2000;44(6):459–478.

3. Zwick H. Visual functional changes associated with low-level light effects. *Health Phys.* 1989;56(5):657–663.

4. Zwick H, Ness JW, Belkin M, Stuck BE. In vivo diagnostics and metrics in the assessment of laser-induced retinal injury. In: Friedl KE, Santee WR, eds. *Military Quantitative Physiology: Problems and Concepts in Military Operational Medicine*. Fort Detrick, MD: Borden Institute; 2012: 129–155.

5. Zwick H, Elliot R, Schuschereba S, Lund D, Stuck B. In vivo confocal scanning laser ophthalmoscopic characterization of retinal pathology in a small-eye-animal model. *Proc SPIE*. 1997;2974:44–50. doi:10.1117/12.275253.

6. Zwick H, Elliot R, Li G, Akers A, Edsall P, Stuck B. In vivo imaging of photoreceptor structure and laser injury pathophysiology in the snake eye. *Proc SPIE.* 1999;359:368–374. doi:10.1117/12.350599.

7. Li G, Zwick H, Tribble J, Ness J, Lund D, Reddix M. On- and off-axis confocal double pass measurements of the point spread function in the human eye. *Proc SPIE.* 1999;3591:351–358. doi:10.1117/12.350596.

8. Masters B, Bohnke M. Three-dimensional confocal microscopy of the living human eye. *Annual Review of Biomedical Engineering*. 2002;4:69–91.

9. McIlwain J. *An Introduction to the Biology of Vision*. New York, NY: Cambridge University Press; 1996.

10. Brodal P. *The Central Nervous System: Structure and Function*. 3rd ed. New York, NY: Oxford University Press, Inc.; 2004.

11. Langus A, Zwick H, Stuck B, Belkin M. Foveal photoreceptor explanation of short-term visual acuity recovery associated with laser-induced foveal damage. *Proc SPIE*. 2003;4953:39–50.

12. Curcio CA, Allen K. Topography of ganglion cells in human retina. *J Comp Neurol.* 1990;300(1):5–25.

13. Curcio CA, Kimberly AA, Sloan KR, et al. Distribution and morphology of human cone photoreceptors stained with anti-blue opsin. *J Comp Neurol*. 1991;312:610–624.

14. Zwick H, Stuck B, Dunlap W, Scales D, Lund D, Ness J. Accidental bilateral Q-switched neodymium laser exposure: treatment and recovery of visual function. *SPIE.* 1998;3254:80–89.

15. Breitmeyer B, Valberg A. Local foveal inhibitory effects of global peripheral excitation. *Science.* 1979;203:463–464.

16. Allen D. Fourier analysis and the Farnsworth-Munsell 100-Hue test. *Ophthalmic and Physiol Opt.* 1985;5(3):337–342.

17. Zwick H, Bedell RB, Bloom KR. Spectral and visual deficits associated with laser irradiation. *Mod Probl in Ophthalmol*. 1974;13:299–306.

18. Zwick H, Bloom KR, Beatrice ES. Permanent visual change associated with punctate foveal lesions. In: Drum B, Berries G, eds. *Colour Vision Deficiencies IX*. Documenta Ophthalmologica Proceedings Series, vol 52. Dordrecht, The Netherlands: Kluwer Academic Publishers;1989: 251–260.

19. Arden GB, Grundez K, Perry S. Colour vision testing with a computer graphics system. *Clin Vis Sci*. 1988;2:303–320.

20. Rabin J. Cone specific measures of human color vision. *Invest Ophthalmol Vis Sci.* 1996;37(13):2771–2774.

21. Gunzenhauser J. *Issues in the Development of the Aidman Vison Screener*. Presidio of San Francisco, CA: Letterman Army Institute of Research; 1990. http://www.dtic.mil/dtic/tr/fulltext/u2/a232777.pdf. Accessed July 10, 2018.

22. Ness J, Zwick H, Stuck B, et al. Retinal image motion during deliberate fixation: implications to laser safety for long duration viewing. *Health Phys.* 2000;78(2):131–142.

23. Zwick H, Stuck B, Gagliano D, et al. *Two Informative Cases of Q-Switched Laser Eye-Injury*. Presidio of San Francisco, CA: Letterman Army Institute of Research; 1991. Institute Report No. 463.

24. Stuck B, Zwick H, Molchany J, Lund D, Gagliano D. Accidental human laser retinal injuries from military laser systems. *SPIE.* 1996;2674:7–20.

25. Robson JG. Spatial and temporal contrast sensitivity functions of the human visual system. *J Opt Soc Am.* 1966;56:1141–1142.

26. Chatterjee S, Callaway E. S cone contributions to the magnocellular visual pathway in macaque monkey. *Neuron.* 2002;35:1135–1146.

27. Frisch G, Shawaluk P, Adams D. Remote nerve fibre bundle alterations in the retina caused by argon laser photocoagulation. *Nature.* 1974;248: 433–435.

28. Zwick H, Belkin M, Zuclich JA, Lund DJ, Schuschereba S, Scales D. Laser-induced retinal nerve fiber layer injury in the nonhuman primate. In: Stuck BE, Belkin M, eds. *Laser-Inflicted Eye Injuries: Epidemiology, Prevention, and Treatment. Proc SPIE.* 1995;2674:89–96.

29. Ness J, Zwick H, Lund B, Brown J, Stuck B. Fixational eye movement patterns reflect macular pathology induced by accidental laser exposure. *Invest Ophthalmol Vis Sci.* 2000;41(4). Abstract 4323-B270.

30. Brown J, Zwick H, Schuschereba ST, Stuck BE. Clinical features of laser-induced macular holes as imaged by optical coherence tomography (OCT). *Proc SPIE*. 2001;4246:10–19.

31. Custis P, Gagliano D, Zwick H, Schuschereba S. Macular hole surgery following accidental laser injury with a military rangefinder. *SPIE.* 1996;2674:166–174.

32. Zwick H, Ness J, Molchany J, Stuck B, Loveday J. Neural motor ocular strategies associated with the development of a pseudo fovea following laser-induced macular damage and artificial macular occlusion: is the fovea replaceable? *J Laser Appl*. 1998;10:144–147.

33. Zwick H, Stuck B, Brown J, Ness J, Scales D. Long-term evaluation of two bilateral laser eye accident cases. *Proc ILSC.* 1999;113–122.

34. Zwick H, Lund BJ, Brown J Jr, Stuck BE, Loveday J. Human color vision deficits induced by accidental laser exposure and potential long-term recovery. *Proc SPIE*. 2003;4953:27–39. doi:10.1117/12.488645.

35. Stuck B, Zwick H, Scales D, Ness J, Brown J. Preferred retinal location (PRL) in two long- term human laser eye accident cases. *Invest Ophthalmol Vis Sci.* 1999;40(4):S954.

36. Enoch J, Van Loo J, Okun E. Realignment of photoreceptors disturbed in orientation secondary to retinal detachment. *Invest Ophthalmol Vis SCI.* 1973;12:849–853.

37. Gilbert C, Wiesel T. Receptive field dynamics in adult primary visual cortex. *Nature.* 1992;356(6365):150–152.

38. Jenkin M, Harris L. *Seeing Spatial Form*. New York, NY: Oxford University Press; 2006.

39. Zwick H, Lund B, Brown J, Stuck B, Loveday J. Human color vision deficits induced by accidental laser exposure and potential for long-term recovery. *Proc SPIE.* 2003;4953:27–39. doi:10.1117/12.488645.

40. Robbins DO, Zwick H. Subthreshold functional additivity occurring at the transition zones between temporary and permanent laser-induced visual loss. *Proc SPIE.* 1996;2674:44–61.

41. Sperling HG, Johnson C, Harwerth RS. Differential spectral photic damage to primate cones. *Vision Res.* 1980; 20(12):1117–1125.

42. Ham WT, Mueller HA, Sliney DH. Retinal sensitivity to damage from short wavelength light. *Nature.* 1976;11:153–155.

43. Reidenbach H-D, Beckmann D, Al Ghouz I, Dollinger K, Ott G, Brose M. Is there an unknown risk for short-wavelength visible laser radiation? *Strahlenschutzpraxis (Koeln).* 2013;19(3):45U–53.

44. Stamper DA, Lund DJ, Molchany JW, Stuck BE. Laser-Induced afterimages in humans. *Percept Mot Skil.* 2000;91:15–33.

45. Zuclich JA. Ultraviolet-induced photochemical damage in ocular tissue. *Health Phys.* 1989;56(5):671–682.

46. Glickman RD. Phototoxicity to the retina: mechanisms of damage. *Int J Toxicol*. 2002;21:473–490.

47. Dormidonov AE, Kompanets VO, Chekalin SV, Kandidov VP. Giantically blue-shifted visible light in femtosecond mid-IR filament in fluorides. *Opt Express*. 2015;23(22):29202–29210.

48. Schmeisser E. Laser flash effects on laser speckle shift VEP. *Am J Optom Physiol Opt*. 1985;62(10):709–714.

49. Schuschereba S, Zwick H, Stuck BE, Beatrice ES. *Basal Body and Striated Rootlet Changes in Primate Macular Retinal Pigmented Epithelium After Low Level Diffuse Argon Laser Radiation.* Presidio of San Francisco, CA: Letterman Army Institute of Research. LAIR 82-35TN; 1982:1–19. DTIC OCLS#227557021.

50. Zwick H, Edsall P, Stuck B, et al. Laser-induced photoreceptor damage and recovery in the high numerical aperture eye of the garter snake. *Vision Res.* 2008;48(3):486–493.

51. Li G, Zwick H, Stuck B, Lund D. On the use of schematic eye models to estimate image quality. *J Biomed Opt*. 2000;5(3):307–314.

52. Tso MO, Robbins DO, Zimmerman LE. Photic maculopathy. A study of functional and pathologic correlation. *Mod Probl Ophthalmol*. 1974;4:220–228.

53. Westheimer G. Directional sensitivity of the retina: 75 years of Stiles-Crawford effect. *Proc R Soc Biol Sci*. 2008;275:2777–2786.